Selection of damage-sensitive features based on probability of detection curves

Alexander Mendler, Michael Döhler, Christian U. Grosse

9th International Operational Modal Analysis Conference
iomac
July 3 - 6, 2022
Vancouver, Canada

SELECTION OF DAMAGE-SENSITIVE FEATURES BASED ON PROBABILITY OF DETECTION CURVES

Alexander Mendler[1], *Michael Döhler*[2], *Christian U. Grosse*[3]

[1] Postdoctoral Fellow, Technical University of Munich, TUM School of Engineering and Design, Munich, Germany, alexander.mendler@tum.de

[2] Research Scientist, Univ. Gustave Eiffel, Inria, COSYS/SII, I4S, Rennes, France, michael.doehler@inria.fr

[3] Professor, Technical University of Munich, TUM School of Engineering and Design, Munich, Germany, grosse@tum.de

ABSTRACT

The first phase of each structural monitoring project is the operational evaluation. Its purpose is to define relevant damage mechanisms and environmental conditions, to consider the data acquisition limitations on site, and to justify the investment. Subsequently, relevant measurement quantities and damage-sensitive features are selected, but very few systematic approaches exist in the literature on how to select the most appropriate features. The presented paper fills this gap and develops an approach to select damage-sensitive features based on probability of detection (POD) curves. The POD curves are generated based on a novel method for statistical damage detection tests that requires a finite element model and vibration data from the undamaged structure. However, no data is required from the damaged state, making it particularly suited for unique or large and complex engineering structures. The approach explicitly considers the uncertainties in the features due to unknown loads, measurement noise, and short measurement durations. Although global damage-sensitive features are considered, such as modal parameters and subspace-based residuals, the detectability is evaluated for local structural components. The paper includes a proof of concept study on a laboratory structure. The results demonstrate that the developed method successfully finds the feature with the highest damage detectability for a chosen damage scenario, and that the detectability varies depending on the monitored local component.

Keywords: Structural health monitoring, ambient vibrations, Fisher information, probability of detection

1. INTRODUCTION

National building standards require visual inspections and non-destructive testing for critical engineering structures in periodic intervals. Increasingly, structural health monitoring (SHM) system are installed, meaning sensors are permanently installed on the structure and online damage diagnosis algorithms are

trained to automatically diagnose damages in-between the scheduled inspections. The four main stages of each SHM project are the operational evaluation, the data acquisition, the extraction of damage-sensitive features (such as natural frequencies or mode shapes), and their statistical evaluation [1]. Each phase exhibits distinct challenges, for example, the correct parametrization of damage, the selection of appropriate measurement quantities and sensor locations, and the selection of appropriate damage-sensitive features, and algorithms.

Feature selection is a critical topic. Some machine learning experts prefer a 'blind' feature selection, for example, based on neuronal networks whose training process can involve the automated selection of features. Others prefer a 'manual' selection based on engineering judgement, experiences with similar structures, or analytical and structure-specific approaches. Such analytical approaches include sensitivity analyses using finite element models [1], where the effect of individual parameter changes on the data-driven features is studied, or approaches based on confidence intervals, where the changes in the features is put into relation to the statistical uncertainties that are inherent to the features' estimation process. However, few method-specific approaches exist to select the feature with the highest damage detectability. A novel idea is to select features based on probability of detection (POD) curves for critical damage scenarios, as they quantify the reliability of a SHM system. POD curves are standard approaches to verify the effectiveness of non-destructive testing [2], but they are rarely used in SHM. The reason for this is that most methods (e.g., the 29-29 method, the $\hat{a}$ vs. a method, the hit/miss method, the delta method, Bayesian approaches) require empirical data from the damaged state, and this data is typically not available for large and unique structures, such as bridges, highrises, and dams. The main idea of this article is to propose a new method for the creation of POD curves that does not require empirical data from damaged structures. The second objective is to apply this approach to various features and to select the feature that exhibits the highest damage detectability.

The paper is organized as follows: Section 2. recaps state-of-the-art vibration models. Section 3. explains how damage-sensitive features can be formed based on the dynamic system properties, how they can be evaluated statistically, and how POD curves can be predicted based on measurement data from undamaged structures. Section 4. showcases a proof of concept study based on a laboratory beam with extra masses, and Section 5. summarizes the main findings.

2. BACKGROUND

The presented approach is applied to vibration-based features and requires in-depth knowledge on operational modal analysis. This section recaps how modal parameters can be obtained from measurement data using subspace-based system identification. All following considerations are based on linear and time-invariant dynamic systems with m degrees of freedom (DOF)

$$\mathbf{M}\ddot{\mathbf{u}} + \mathbf{D}\dot{\mathbf{u}} + \mathbf{K}\mathbf{u} = \mathbf{f}, \tag{1}$$

where $\mathbf{M}, \mathbf{D}$ and $\mathbf{K}$ are the mass, damping, and stiffness matrices $\mathbb{R}^{m\times m}$, $\mathbf{u} \in \mathbb{R}^m$ is the displacement vector, and $\mathbf{f} \in \mathbb{R}^m$ is the force vector. Sampling the displacement vector at Δt and substituting the state vector $\mathbf{x}_k = \begin{bmatrix}\mathbf{u}(k\Delta t)^T & \dot{\mathbf{u}}(k\Delta t)^T\end{bmatrix}^T \in \mathbb{R}^n$, the model is transformed to a discrete-time state space model, with $n = 2m$,

$$\begin{cases} \mathbf{x}_{k+1} &= \mathbf{A}\mathbf{x}_k + \mathbf{w}_k \\ \mathbf{y}_k &= \mathbf{C}\mathbf{x}_k + \mathbf{v}_k \end{cases} \tag{2}$$

where $\mathbf{A} \in \mathbb{R}^{n\times n}$ is the state transition matrix, $\mathbf{C} \in \mathbb{R}^{N_{ch}\times n}$ is the output matrix and N_{ch} is the number of measurement channels. The term $\mathbf{y}_k$ is the output vector, and $\mathbf{w}_k$ and $\mathbf{v}_k$ state noise and measurement noise. [3]

2.1. Subspace Decomposition

The first step is to acquire output data $\mathbf{Y} = [\mathbf{y}_1 \ \mathbf{y}_2 \ \dots \ \mathbf{y}_N]^T \in \mathbb{R}^{N \times N_{ch}}$ (displacements, velocities, or accelerations), where N is the number of data points and N_{ch} is the number of measurement channels. Next, output covariance functions are evaluated $\mathbf{R}_i = \frac{1}{N-i} \sum_{k=1}^{N-i} \mathbf{y}_{k+i} \mathbf{y}_k^T$ and arranged in a block Hankel matrix, i.e., a matrix with identical blocks on the anti-diagonals

$$\boldsymbol{\mathcal{H}}_{p+1,q} = \begin{bmatrix} \mathbf{R}_1 & \mathbf{R}_2 & \dots & \mathbf{R}_q \\ \mathbf{R}_2 & \mathbf{R}_3 & \dots & \mathbf{R}_{q+1} \\ \vdots & \vdots & \ddots & \vdots \\ \mathbf{R}_{p+1} & \mathbf{R}_{p+2} & \dots & \mathbf{R}_{p+q} \end{bmatrix} = \begin{bmatrix} \mathbf{U}_1 & \mathbf{U}_0 \end{bmatrix} \begin{bmatrix} \mathbf{S}_1 & \mathbf{0} \\ \mathbf{0} & \mathbf{S}_0 \end{bmatrix} \begin{bmatrix} \mathbf{V}_1^T \\ \mathbf{V}_0^T \end{bmatrix}, \tag{3}$$

where p and q are time lag parameters. Thirdly, singular value decomposition (SVD) is applied to the block Hankel matrix, and the resulting quantities are truncated at the presumed model order, determined through the m physical modes of vibration, yielding the first $n = 2m$ singular values in $\mathbf{S}_1$ and the corresponding singular vectors $\mathbf{U}_1$ (the column space). The remaining singular values $\mathbf{S}_0$ contain noise with the corresponding left null space vectors in $\mathbf{U}_0$.

2.2. Modal Identification

This section revisits how modal parameters can be derived from the block Hankel matrix [3]. First, the observability matrix $\boldsymbol{\mathcal{O}}_{p+1}$ is constructed based on the first n singular values and the column space

$$\boldsymbol{\mathcal{O}}_{p+1} = \mathbf{U}_1 \mathbf{S}_1^{1/2}. \tag{4}$$

The output matrix $\mathbf{C}$ can be extracted from the observability in Eq. (4) as the first block row, and the state transition matrix can be approximated through regression, using the shift-invariance property [4]

$$\mathbf{A} = (\boldsymbol{\mathcal{O}}_{p+1}^{\uparrow})^{\dagger} \boldsymbol{\mathcal{O}}_{p+1}^{\downarrow}, \tag{5}$$

where $\boldsymbol{\mathcal{O}}_{p+1}^{\uparrow}$ and $\boldsymbol{\mathcal{O}}_{p+1}^{\downarrow}$ denote the observability matrix without the last and without the first block row, respectively. Modal parameters can be estimated by solving the eigenvalue problem $\mathbf{A}\boldsymbol{\Phi} = \boldsymbol{\Phi}\boldsymbol{\Lambda}$. Eigenvalues occur in complex conjugate pairs $\boldsymbol{\Lambda} = \boldsymbol{\Phi}^{-1}\mathbf{A}\boldsymbol{\Phi} = \mathrm{diag}(\lambda_1, \bar{\lambda}_1 \dots, \lambda_n, \bar{\lambda}_n)$ and so do the eigenvectors. Ultimately, natural frequencies and mode shapes are calculated as follows

$$\mu_j = \frac{\log \lambda_j}{\Delta t}, \quad f_j = \frac{|\mu_j|}{2\pi}, \qquad \boldsymbol{\Psi} = \mathbf{C}\boldsymbol{\Phi} = \begin{bmatrix} \boldsymbol{\Psi}_1 & \cdots & \boldsymbol{\Psi}_n \end{bmatrix}. \tag{6}$$

2.3. Mode Shape Normalization

Mode shapes are unique dynamic properties up to a scaling factor. To enable a comparison of mode shapes, they have to be normalized, e.g., to unit displacement of one of its components l,

$$\bar{\boldsymbol{\Psi}}_i = \frac{1}{\max\{|\Psi_{i,l}|\}} \cdot \boldsymbol{\Psi}_i. \tag{7}$$

This forces the maximum amplitude of each normalized mode shape to be equal to one (even when damage has occurred). Consequently, the maximum mode shape component carries no damage-related information after scaling and the mode shape dimension might as well be reduced to $\bar{\boldsymbol{\Psi}}^{red} \in \mathbb{R}^{N_{ch}-1 \times m}$, which is done in this paper.

3. METHODOLOGY

3.1. Data-driven Residuals

This section shows a selection of damage-sensitive residuals that can be formed based on dynamic system properties from the previous section. In the subsequent sections, the POD curves will be constructed

for all features presented in this section. For example, the natural frequencies could be extracted and compared to the baseline values from the training phase

$$\mathbf{r}_1 = \mathbf{f} - \mathbf{f}^0, \tag{8}$$

where the number of entries in the residual vector depends on the number of observed modes of vibration. Another example is the mode shape residual. To reduce the mode shape matrix into a single vector, the vectorization operator $\text{vec}(\cdot)$ is used and all matrix columns are stacked

$$\mathbf{r}_2 = \text{vec}(\bar{\mathbf{\Phi}}^{red}) - \text{vec}(\bar{\mathbf{\Phi}}^{red,0}), \tag{9}$$

where the number of residual entries now depends on the number of modes of vibration and the number of sensors. Since modal frequencies and mode shapes are the results from the same estimation procedure, they can (and should) also be analyzed simultaneously, using a modal vector $\boldsymbol{\eta}$ with the corresponding residual

$$\mathbf{r}_3 = \boldsymbol{\eta} - \boldsymbol{\eta}^0, \quad \text{where} \quad \boldsymbol{\eta} = \begin{bmatrix} \mathbf{f} \\ \text{vec}(\bar{\mathbf{\Phi}}^{red}) \end{bmatrix}. \tag{10}$$

The last considered residual is the subspace-based residual. It takes advantage of the orthogonality between the left null space singular vectors and the block Hankel matrix in the reference state [5]

$$\mathbf{r}_4 = \text{vec}(\mathbf{U}_0^T \boldsymbol{\mathcal{H}}_{p+1,q}) \tag{11}$$

and its size depends on the time lag parameters p and q.

3.2. Damage Detection

This section summarizes the specific damage diagnosis method for which the POD curves are constructed. In this paper, structural changes are analyzed based on a parametrized statistical test, i.e., a statistical test on data-driven residuals that is linked to structural models through sensitivity vectors. The test statistic is defined as [5]

$$t = N \cdot \mathbf{r}^T \mathbf{\Sigma}^{-1} \boldsymbol{\mathcal{J}} \left(\boldsymbol{\mathcal{J}}^T \mathbf{\Sigma}^{-1} \boldsymbol{\mathcal{J}} \right)^{-1} \boldsymbol{\mathcal{J}}^T \mathbf{\Sigma}^{-1} \mathbf{r}, \tag{12}$$

where N is the sample size during testing, $\mathbf{r}$ is one of the damage-sensitive residual vectors from Section 3.1., $\boldsymbol{\mathcal{J}}$ is the first-order derivative of the residual with respect to structural design parameters $\boldsymbol{\theta}$

$$\boldsymbol{\mathcal{J}} = \left. \frac{\partial E_{\boldsymbol{\theta}}[\mathbf{r}]}{\partial \boldsymbol{\theta}} \right|_{\boldsymbol{\theta}=\boldsymbol{\theta}^0}, \tag{13}$$

and $\mathbf{\Sigma}$ is the sample covariance of the damage-sensitive residual which, when evaluated on n_b datasets of length N, is defined as

$$\mathbf{\Sigma} = \frac{N}{n_b - 1} \sum_{k=1}^{n_b} \mathbf{r}_k \, \mathbf{r}_k^T. \tag{14}$$

Structural parameters $\boldsymbol{\theta} \in \mathbb{R}^H$ typically include material properties, cross-sectional values, prestressing forces, or geometric properties of the structure that manifest damage. Defining the relevant damage parameters is part of the first phase of each monitoring phase, the operational evaluation.

The Jacobian matrix $\boldsymbol{\mathcal{J}}$ links structural parameter changes and changes in data-driven features through $\mathbf{r} \approx \boldsymbol{\mathcal{J}}\boldsymbol{\theta}$. It can either be approximated using the finite difference method, or it can be calculated analytically. For the subspace-based residual, the analytical calculation is described in [6] and for the modal residuals, typical approaches include the modal approach [7] or Nelson's method [8].

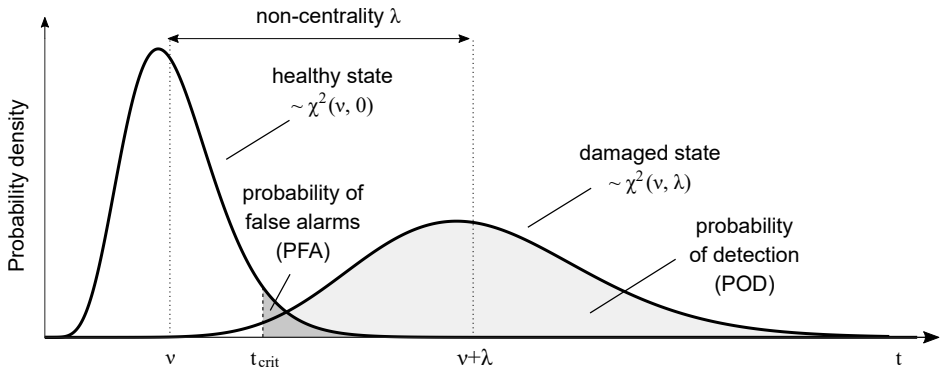

Figure 1: Distribution of the test statistic in the undamaged and damaged state

The covariance matrix is calculated based on data, where the main diagonal holds the variance of each residual entry. It can either be computed empirically based on multiple sets of features from the training phase, or in a combined analytical/empirical approach based on a single measurement record for both the modal residuals [9, 10] and the subspace-based residuals [5, 11].

Uncertainties due to unknown loads and measurement noise cause the test statistic in Eq. (12) to be scattered. Since the damage-sensitive residuals can be approximated by a Gaussian distribution, the tests can be approximated as a chi-squared distribution $\chi^2(\nu, \lambda)$ with $\nu = \text{rank}(\boldsymbol{\mathcal{J}}^T \boldsymbol{\Sigma}^{-1} \boldsymbol{\mathcal{J}})$ degrees of freedom, and non-centrality λ in the damaged state. To make a decision on whether or not the structure is damaged, a safety threshold t_{crit} is introduced, for example, based on the distribution in the undamaged state, and an alarm is issued if the test exceeds the safety threshold, see Fig. 1.

3.3. Probability of Detection Curves

A powerful aspect of the parametric hypothesis tests in Eq. (12) is that the mean test response to a well-defined parameter change can be predicted based on quantities that are available in the undamaged state of the structure. If damage is assumed to be restricted to a single parameter change $\theta_h - \theta_h^0$, the mean test response (the non-centrality) λ is [12]

$$\lambda = N(\boldsymbol{\theta}_h - \boldsymbol{\theta}_h^0)^2 F_{hh}, \qquad F_{hh} = \boldsymbol{\mathcal{J}}_h^T \boldsymbol{\Sigma}^{-1} \boldsymbol{\mathcal{J}}_h, \tag{15}$$

where F_{hh} is the Fisher information and $\boldsymbol{\mathcal{J}}_h$ is the column in the Jacobian matrix that corresponds to the examined parameter θ_h. The larger the mean test response from Eq. (15), the more frequently the test statistic yields values beyond the safety threshold, and the higher the POD. The POD can be quantified as the area under the probability density function of the test statistics beyond the safety threshold, Fig.1,

$$\text{POD} = \int_{t_{crit}}^{\infty} f_{\chi^2}(\nu, \lambda)(t) dt, \tag{16}$$

where the safety threshold could, for example, be defined based on the quantile value of the healthy state distribution of the test statistic. Assuming that the test response λ is known, the formula from Eq. (15) can also be solved for the minimum detectable parameter change

$$\Delta_h = \frac{1}{\theta_h} \sqrt{\frac{\lambda}{N F_{hh}}}. \tag{17}$$

Utlimately, the POD curves can be constructed as follows: First, the non-centrality is fixed to zero $\lambda = 0$. Next, the non-centrality is gradually increased $\lambda = \lambda + \varepsilon$ in steps of ε, while evaluating the POD based on the corresponding probability density function in Eq. (16) and Fig. 1 and the minimum detectable damage Δ_h using Eq. (17). Drawing the POD over Δ_h yields the probability of detection curve for parameter θ_h.

4. APPLICATION

The goal of this section is to analytically construct POD curves based on data from an undamaged structure. Subsequently, actual damage is applied, and it is demonstrated that the empirical POD is close to the analytical one, which was predicted based on undamaged data.

4.1. Laboratory Experiment

The specimen under consideration is a hollow structural steel beam (HSS 152x51x4.78 mm) with a modulus of elasticity of E = 210,000 MPa and a total mass of m = 56.8 kg, Fig. 3. The beam is located at the University of British Columbia and has already been described in the referenced literature [12, 13]. The length of the beam is 4.1 m and pin supports are installed on both ends. The instrumentation consists of eight vertical accelerometers with a weight of 1.28 kg, placed at equal distances, and one shaker with a mass of 3.6 kg and a moving mass of 360 g that injects white noise signals in-between sensors 2 and 3. All other signal processing parameters are given in Table 1.

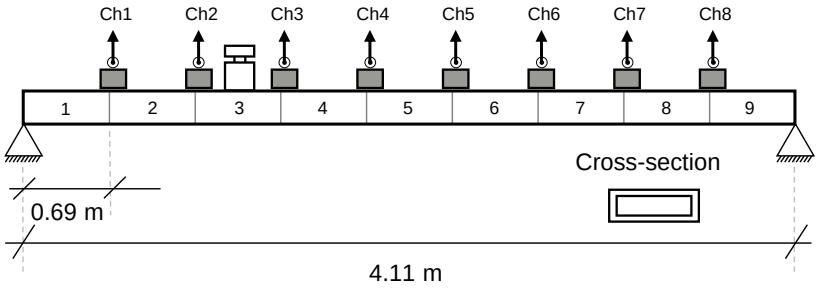

Figure 2: Schematic depiction of the laboratory beam indicating the eight beam segments

Damage is parametrized as a change in mass so the experiments can be conducted non-destructively. A finite element model is built and split into nine beam segments, Fig. 2. Each segment is assigned a different mass value and only mass 8 and 9 are monitored, yielding the parameter vector

$$\boldsymbol{\theta} = \begin{bmatrix} m_8 \\ m_9 \end{bmatrix}. \tag{18}$$

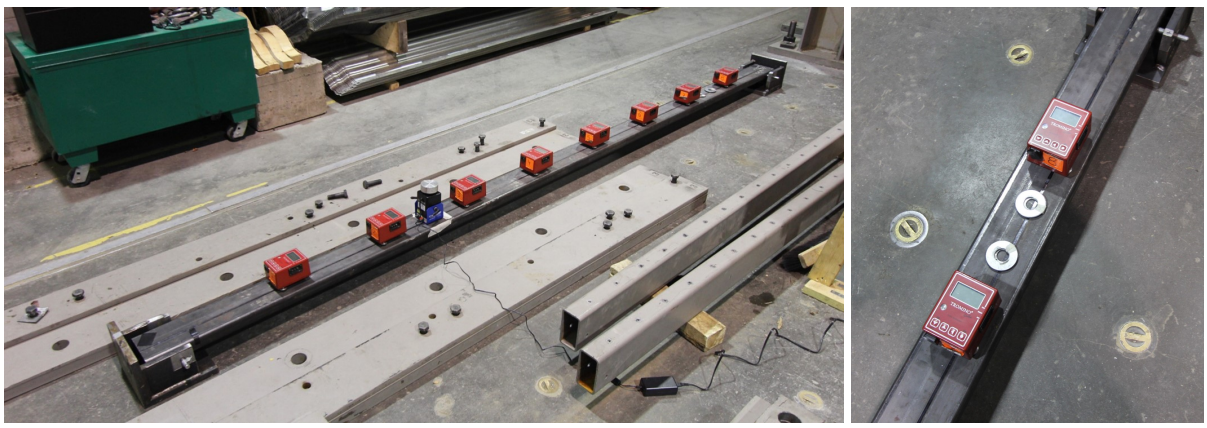

Figure 3: Laboratory HSS beam with eight sensors and one shaker (left) and applied extra masses (right)

4.2. Analytical Results

All studies in this section are based on measurement data from the undamaged structure, where only data from the first four measurement channels is used, Fig. 2. In this state, one long measurement with

Data Acquisition		Data Segmenting	
Measured quantity	acceleration	No. of training segments	100
Sampling frequency	200 Hz	No. of testing segments	100
Reference data length	110 min	Samples/segment	2,000
Testing data length	110 min	Duration/segment	10 s
Modal Parameters		**Subspace-based Residual**	
System order n	14	System order n	14
Time lags p	20	Time lags p	11

Table 1: Data acquisition and signal processing parameters

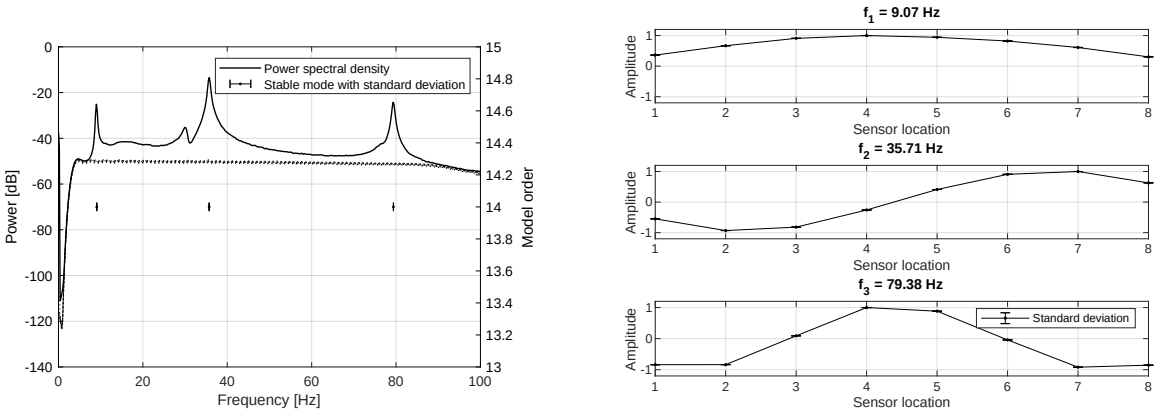

Figure 4: Uncertainty quantification for natural frequencies and mode shapes

a duration of T = 110 min is recorded to be able to estimate the Fisher information, the reference values for the residuals in Section 3.1. (the natural frequencies, the mode shapes, and the nullspace), and the safety thresholds.

The Fisher information $\mathbf{F}$ can be calculated based on the Jacobian matrix $\boldsymbol{\mathcal{J}}$ and the covariance matrix $\boldsymbol{\Sigma}$, see Eq. (15). The covariance matrix is calculated based on [5, 10] and for visualization, the standard deviations of the measured modal parameters (i.e., the square root of the covariance's main diagonal values) are shown in Fig. 4 through error bars. For modal parameters, the Jacobian matrix computation can be done based on the numerical model but for the subspace-based residual, data-driven components have to be considered [6]. Once the Jacobian and the covariance matrix are estimated, the Fisher information can be calculated and the main diagonal values F_{hh} can be extracted.

The last required quantity is the safety threshold value t_{crit}. It is different for each damage-sensitive residual, because the χ^2-distribution exhibits a different number of degrees of freedom. In this study, the thresholds are set based on the 0.1% quantile value of the healthy state distribution, meaning one out of 1,000 test statistics is beyond the safety threshold in the undamaged state. The corresponding safety thresholds are 22 for the subspace-based residual, 16 for the frequency-based residual, 16 for the mode shape-based residual, and 22 for the combined frequency and mode shape-based residual.

With the Fisher information and the safety threshold at hand, the POD curves can be predicted for all damage-sensitive residuals from Eq. (8)-(11) with the results being displayed in Fig. 5. The POD curves are drawn for each monitoring parameter, i.e., for parameter 8 and 9 from Eq. (18). The first observation is that changes in parameter 8 lead to a much higher POD than in parameter 9, meaning the damage detectability close to the support is small. According to the POD curves for parameter 8, the frequency-based residual is the most sensitive to changes in the eighth mass parameter, as a parameter change of $\Delta\theta_8 = 5\%$ already leads to a POD close to 87%. The mode shape-based residual, on the other hand,

is the least sensitive and a parameter change of 5% leads to a POD of close to 0%, and the subspace-based residual leads to a POD of about 20%. It should be noted that the POD curves are created for particular damage scenarios, captured through the parameter vector in Eq. (18). It appears that the mode shapes do not change for mass changes in beam segment eight and nine, but for other scenarios, they may significantly contribute to the damage detectability and should therefore be considered.

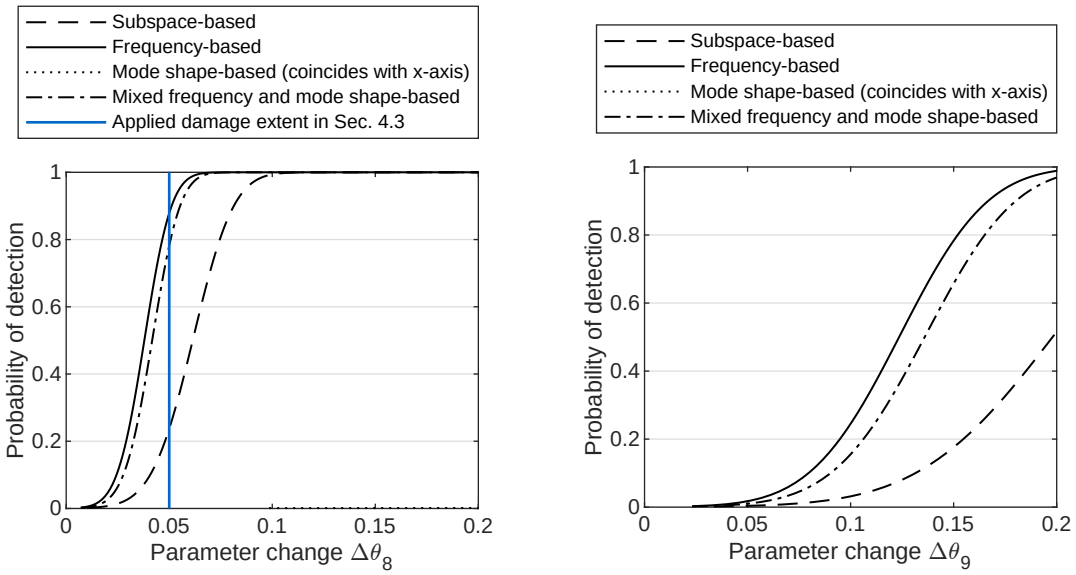

Figure 5: Predicted POD curves based on data from the undamaged state for extra masses on beam segment 8 (left) and beam segment 9 (right) for different residual formulations from Section 3.1

4.3. Empirical Validation

In this section, data from the damaged structure is analyzed for the first time to validate the predictions that were made based on data from the undamaged state. The main idea is to apply a 5% mass increase to the eighth beam segment, simply by placing two washers on top of the beam between sensors seven and eight (see Fig. 3, right side), and to verify whether the empirically evaluated POD is close to the predicted ones from Fig. 5. To evaluate the POD empirically, the test statistic is applied to 100 data sets from the damaged structure, with a measurement duration of 10 s for each segment, and the relative number of tests beyond the safety threshold is counted.

For the frequency-based residual, the empirically evaluated POD is 81.1%, Fig. 6, which is very close to the analytical value of 87%. Likewise, the mode shape-based residual leads to a POD of 0% and the subspace-based residual exhibits a POD of 19.4%, as predicted in Fig. 5. This concludes the validation study, as the analytical POD curves predict the empirical POD for all residuals with sufficient accuracy.

4.4. Discussion

Safety threshold. A peculiar observation appears to be that, in some cases, the mixed frequency and mode shape-based residual leads to a lower POD than the frequency-based residual although more information is available from the structure, see Fig. 5. The reason for this is that the frequency-based residual exhibits a narrower distribution in the undamaged state and a lower safety threshold value of 16 instead of 22. Therefore, an equivalent mean test response leads to a higher POD.

Sensor layout. The study in the previous section concluded that the frequency-based residual is more sensitive to damage than the subspace-based residual. It is important to understand that this result is only valid for the considered sensor layout, because both the sensitivity and the covariance of extracted features depend on the sensor location. To emphasize this, Fig. 7 shows how the POD curves change if the number of channels is increased from 4 to 8. Consequently, the number of mode shape coordinates

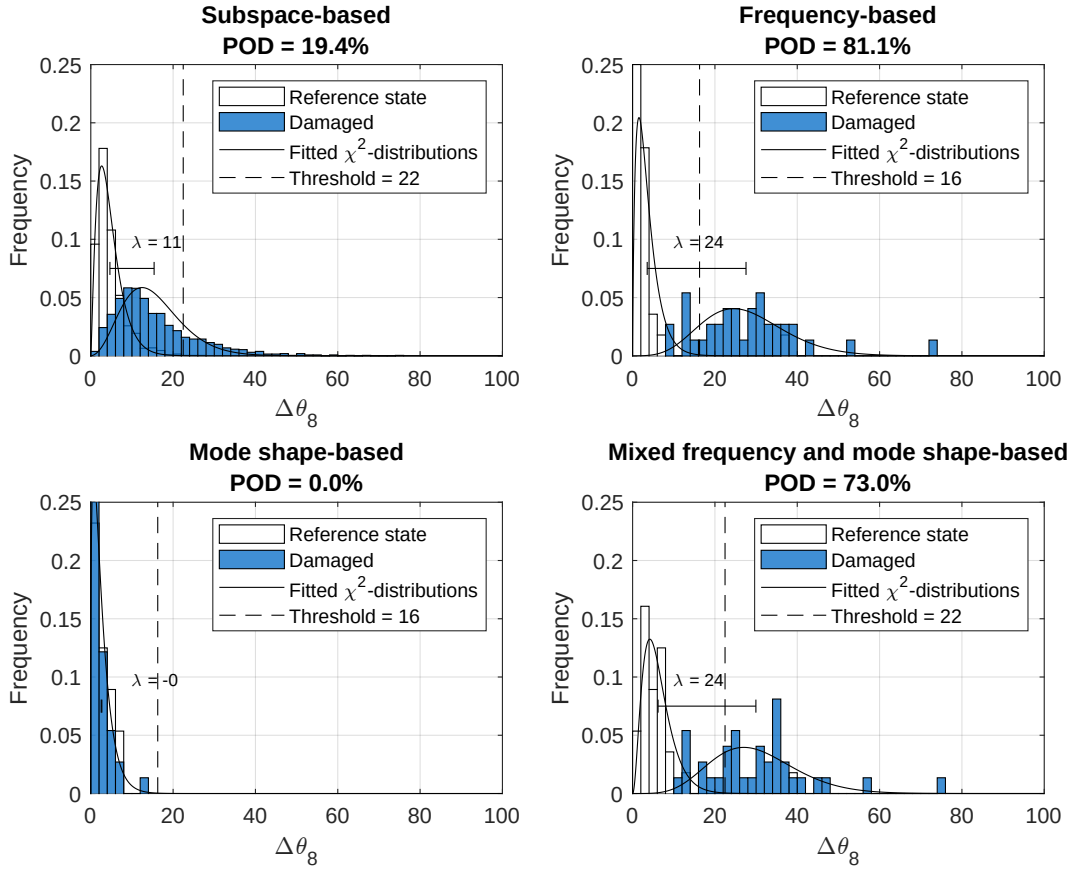

Figure 6: Damaged state: Comparing the empirical POD for different residual formulations from Section 3.1

increases and the POD for the mode shaped-based residual increases for large parameter changes. At the same time, the POD of the subspace-based residual increases from 20% (Fig. 5 left) to almost 100% (Fig. 7 left), making it more sensitive to damage than the frequency-based residual. In other words, the POD curves are powerful means for sensor placement optimization. A systematic approach to optimize the sensor layout can be found in [13].

Measurement noise. One of the advantages of the developed approach is that the uncertainties in the feature due to measurement noise is explicitly considered in the covariance matrix, without having to measure the signal-to-noise ratio. To demonstrate this, vibration data is numerically generated and different noise levels are added to the vibrations. Fig. 7 shows the POD curves for two cases, the mode shape-based residual with a measurement noise level that corresponds to 5% and 10% of the output signal's variance. For the damage scenario $\Delta\theta_8 = 5\%$, the POD increases from about 0% to 12% due to decreased noise level. For other residual formulations considered in this paper, the POD changed as well but the mode shape-based residual appears to be particularly sensitive to measurement noise.

Spatial information. Since POD curves can be evaluated for different structural parameters, they carry spatial information. However, they should not be considered probability of localization (POL) curves, because the statistical test from Eq. (12) is not capable of localizing damage. More advanced statistical tests can identify the parameter that has changed and an approach to determine POL curves can be found in the referenced literature [14].

5. CONCLUSIONS

The main contribution of this paper is an approach to construct probability of detection curves, based on statistical tests and a finite element model. Advantages over other approaches are that no data from the damage state is required and the probability of detection can be analyzed based on data from undamaged

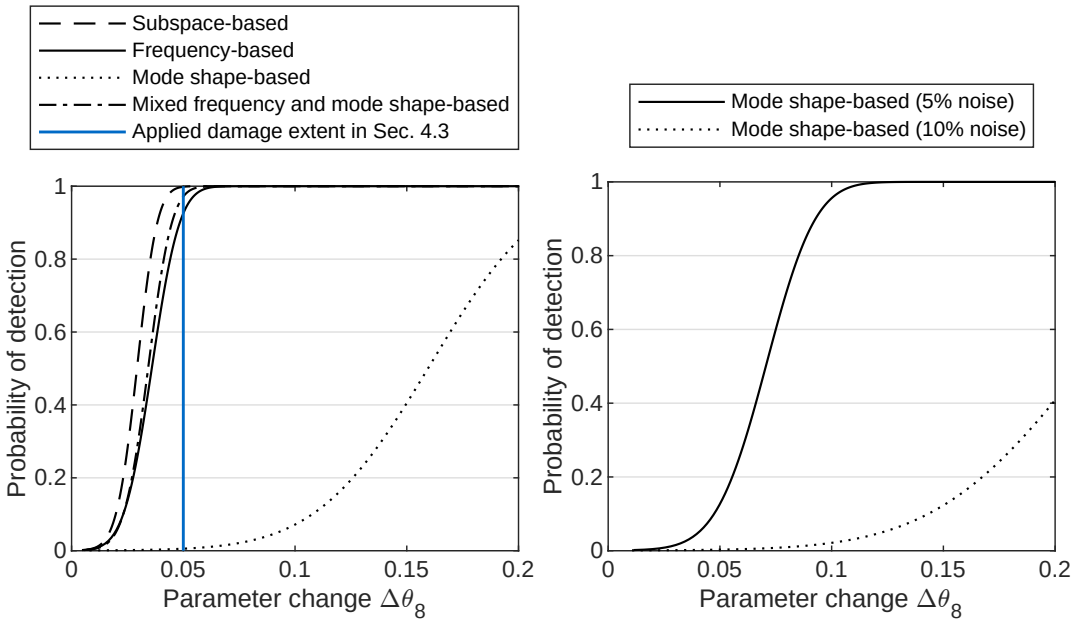

Figure 7: POD curve based on measurement data for an increased number of measurement channels (left), and based on simulated data with varying levels of measurement noise (right).

structures. Moreover, the POD curves can be drawn for different structural parameters, so they include spatial information.

Secondly, it was shown that the developed method for POD curves is a powerful means for feature selection, as features with the highest damage detectability can be chosen before damage occurs. In this paper, the approach is applied to natural frequencies, mode shapes, combined frequency and mode shapes formulations, and the subspace-based residual, but many more features could be incorporated in the framework.

A laboratory case study demonstrates that the POD curves are accurate, even for real data and noisy measurement environments. The main findings are that the POD depends on the structural parameter that is monitored, the sensor layout, and the measurement noise levels. The effect of measurement noise appears to be particularly pronounced for mode shape testing, highlighting the importance of uncertainty quantification in structural health monitoring in general.

An interesting future research topic is the extension to additional features as well as a thorough investigation of measurement noise properties. If measurement noise is modelled accurately, POD curves could be constructed based on numerically generated data and findings can be transferred to real structures.

ACKNOWLEDGMENTS

This research study is funded by dtec.bw – Digitalization and Technology Research Center of the Bundeswehr. The vibration data was kindly provided by Dr. Carlos E. Ventura from the University of British Columbia, Canada.

REFERENCES

[1] Farrar, C., & Worden, K. (2012). *Structural health monitoring: A machine learning perspective*. Wiley, Oxford, U.K.

[2] Berens, A. P. (1989). *NDE Reliability Data Analysis–Metals Handbook*. ASM International, United States.

[3] van Overschee, P., & de Moor, B. (1995). *Subspace identification for linear systems: Theory, Implementation, Application*. Kluwer Academic Publishers, Boston/London/Dordrecht.

[4] Magalhães, F., & Cunha, Á. (2011). Explaining operational modal analysis with data from an arch bridge. *Mechanical Systems and Signal Processing*, *25*(5), 1431–1450.

[5] Basseville, M., Abdelghani, M., & Benveniste, A. (2000). Subspace-based fault detection algorithms for vibration monitoring. *Automatica*, *36*(1), 101–109.

[6] Allahdadian, S., Döhler, M., Ventura, C., & Mevel, L. (2019). Towards robust statistical damage localization via model-based sensitivity clustering. *Mechanical Systems and Signal Processing*, *134*, 106341.

[7] Fox, R., & Kapoor, M. (1968). Rates of change of eigenvalues and eigenvectors. *AIAA journal*, *6*(12), 2426–2429.

[8] Nelson, R. B. (1976). Simplified calculation of eigenvector derivatives. *AIAA journal*, *14*(9), 1201–1205.

[9] Reynders, E., Pintelon, R., & De Roeck, G. (2008). Uncertainty bounds on modal parameters obtained from stochastic subspace identification. *Mechanical systems and signal processing*, *22*(4), 948–969.

[10] Döhler, M., & Mevel, L. (2013). Efficient multi-order uncertainty computation for stochastic subspace identification. *Mechanical Systems and Signal Processing*, *38*(2), 346–366.

[11] Viefhues, E., Döhler, M., Hille, F., & Mevel, L. (2022). Statistical subspace-based damage detection with estimated reference. *Mechanical Systems and Signal Processing*, *164*, 108241.

[12] Mendler, A., Döhler, M., & Ventura, C. E. (2021). A reliability-based approach to determine the minimum detectable damage for statistical damage detection. *Mechanical Systems and Signal Processing*, *154*, 107561.

[13] Mendler, A., Döhler, M., & Ventura, C. E. (2022). Sensor placement with optimal damage detectability for statistical damage detection. *Mechanical Systems and Signal Processing*, *170*, 108767.

[14] Mendler, A., Greś, S., Döhler, M., & Kessler, S. On the probability of localizing damages based on mode shape changes. In: *Proceedings of the EWSHM - European Workshop for Structural Health Monitoring*. Palermo, Italy, July, 2022.